Journal of Alloys and Compounds 586 (2014) 507–511

Contents lists available at ScienceDirect

Journal of Alloys and Compounds

journal homepage: www.elsevier.com/locate/jalcom

High-yield water-based synthesis of truncated silver nanocubes

Yun-Min Chang, I-Te Lu, Chih-Yuan Chen, Yu-Chi Hsieh, Pu-Wei Wu *

Department of Materials Science and Engineering, National Chiao Tung University, Hsin-Chu 300, Taiwan, ROC

ARTICLE INFO

Article history:
Received 15 June 2013
Received in revised form 27 September 2013
Accepted 6 October 2013
Available online 23 October 2013

Keywords:
Silver nanoparticles
Truncated nanocubes
Hydrothermal synthesis
CTAB
Glucose reduction

ABSTRACT

A high-yield water-based hydrothermal synthesis was developed using silver nitrate, ammonia, glucose, and cetyltrimethylammonium bromide (CTAB) as precursors to synthesize truncated silver nanocubes with uniform sizes and in large quantities. With a fixed CTAB concentration, truncated silver nanocubes with sizes of 49.3 ± 4.1 nm were produced when the molar ratio of glucose/silver cation was maintained at 0.1. The sample exhibited (100), (110), and (111) planes on the facets, edges, and corners, respectively. In contrast, with a slightly larger glucose/silver cation ratio of 0.35, well-defined nanocubes with sizes of 70.9 ± 3.8 nm sizes were observed with the (100) plane on six facets. When the ratio was further increased to 1.5, excess reduction of silver cations facilitated the simultaneous formation of nanoparticles with cubic, spherical, and irregular shapes. Consistent results were obtained from transmission electron microscopy, scanning electron microscopy, X-ray diffraction, and UV–visible absorption measurements.

1. Introduction

The synthesis of metallic nanoparticles has been an important research topic with respect to both scientific curiosity and industrial applications [1]. This interest exists because metals in the nanometer size regime not only exhibit unique physical properties due to the quantum confinement effect, but also provide enhanced activities as catalysts and biosensors because of their large surface-to-mass ratio and favorable surface morphology [2–4]. In principle, physical and chemical attributes of metallic nanoparticles are contingent on their size, shape, crystallinity, composition, and structure. Therefore, tailor-made behaviors are feasible if the synthetic steps are controlled deliberately to render nanoparticles with pre-determined specifications. To date, numerous elements, including gold, silver, platinum, and palladium have been prepared in a rich variety of sizes and shapes, and their physical and chemical characteristics have been extensively explored [5–8]. In particular, the formation of silver nanostructures in various forms is critical in applications such as electrocatalysis, water-defouling, and surface-enhanced Raman spectroscopy [9–12].

Silver is a noble metal with a relatively high redox potential. Consequently, the reduction of silver cations is readily induced by external stimuli such as a reducing agent, heat, or photons. In typical wet chemical approaches, a surfactant is usually used to distinguish the growth rate at different crystallographic planes because of its anisotropic adsorption ability. As a result, silver nanostructures in polyhedrons, spheres, cubes, wires, and rods have been demonstrated [13–19]. Earlier, Sun and Xia employed a polyol process to prepare silver nanocubes and used them as a template to produce hollow gold nanoboxes via a displacement reaction [20]. The polyol route involved the use of ethylene glycol (EG) as a reducing agent and solvent; however, the complete removal of EG from the silver nanocubes was difficult. Recently, Yu and Yam reported a water-based hydrothermal process using glucose as a reducing agent other than EG [21]. However, their UV–visible absorption spectra showed a single broad plasma resonance peak, which implied that the resulting samples contained significant numbers of irregular or spherical nanoparticles. Although the non-water-based synthesis of monodispersed silver nanocubes in high yield has been demonstrated, the water-based synthesis of uniform truncated silver nanocubes remains a challenge, and the synthesis method requires further optimization. Moreover, to enable the practical implementation of truncated nanocubes in alkaline fuel cells, the identification of a facile synthesis scheme for their high-yield production is required.

In this work, we design a water-based formulation that enables the fabrication of uniform truncated silver nanocubes in large quantities from a simple hydrothermal process.

2. Experimental

2.1. Materials synthesis

The truncated silver nanocubes were fabricated via a hydrothermal synthetic route using silver nitrate, ammonia, glucose, and cetyltrimethylammonium bromide (CTAB) as precursors. First, 0.17 g of silver nitrate was dissolved in 20 ml of deionized water, followed by the stepwise addition of 1 M ammonia aqueous solution. After the ammonia was added, the transparent silver nitrate solution turned brown briefly, and as the amount of ammonia was increased, the mixture

* Corresponding author. Tel.: +886 3 5131227; fax: +886 3 5724727.
E-mail address: ppwu@mail.nctu.edu.tw (P.-W. Wu).

0925-8388/$ - see front matter © 2013 Elsevier B.V. All rights reserved.
http://dx.doi.org/10.1016/j.jallcom.2013.10.047

appeared transparent again. At this stage, the silver cations were present as $[Ag(NH_3)_2]^+$. Subsequently, we added extra deionized water to render a 10 mM $[Ag(NH_3)_2]^+$ solution. To form the desired silver nanoparticles, 25 ml of 10 mM $[Ag(NH_3)_2]^+$ solution was properly mixed with 15 ml of 50 mM CTAB aqueous solution and 50 ml of glucose aqueous solution. The glucose solution functioned as a reducing agent, and the sample prepared with various concentrations of glucose (i.e., 0.5, 1.75, and 7.5 mM), were designated as SA, SB, and SC, respectively. The CTAB was used as a surfactant for its anisotropic adsorption behavior on distinct crystallographic planes, which allows the silver nuclei to evolve into distinct shapes. The mixture was heated in an autoclave at 120 °C for 8 h and was allowed to cool to 25 °C afterwards. The sample was subsequently centrifuged at 6000 rpm for 20 min to retrieve the silver nanoparticles for characterization and electrochemical analysis.

2.2. Materials characterization

A Siemens D5000 X-ray diffractometer (XRD) equipped with a Cu Kα radiation source ($\lambda = 0.154$ nm) was used to identify relevant phases and preferred orientation. High-resolution images and selective-area electron diffraction patterns were obtained by a transmission electron microscopy (TEM; Philips TECNAI20) to determine the average size and standard deviation, the shape, and the exposed crystallographic planes. We performed UV–visible absorption measurements (JASCO) to explore characteristic plasma resonance peaks. Scanning electron microscopy (SEM; JEOL JSM-6500) was used to directly observe the silver nanoparticles in large quantities and the distribution of silver nanoparticles in working electrodes. The zeta potential of the silver nanoparticles was obtained using a Delsa™ Nano instrument (Beckman Coulter).

3. Results and discussion

Glucose is a known reducing agent with a relatively mild reducing power, and the addition of OH^- is often used to accelerate the reduction reaction [22]. In our case, the reduction of silver ions is further facilitated by an autoclave process at 120 °C for 8 h. The chemical reduction of silver ions by glucose proceeds according to the following equation:

$$CH_2OH{-}(CHOH)_4{-}CHO + 2[Ag(NH_3)_2]^+ + 2OH^- \rightarrow CH_2OH - (CHOH)_4{-}COOH + 2Ag + H_2O + 2NH_3 \quad (1)$$

Fig. 1 provides TEM images of the silver nanoparticles prepared under different synthesis conditions. As shown in Fig. 1a, sample SA consisted of nanoparticles with cubic shapes whose average edge length was 49.3 ± 4.1 nm. In particular, these silver nanocubes also revealed truncated corners and rounded edges. In contrast, in sample SB, as shown in Fig. 1b, the silver nanoparticles exhibited an ideal cubic form with well-defined sharp edges. Their average size, however, was increased to 70.9 ± 3.8 nm. In the case of sample SC, as shown in Fig. 1c, the morphology was notably altered, and cubic, spherical, and irregular-shaped nanoparticles were simultaneously present; the size distribution became slightly wider than those in the other two samples. On average, the particles exhibited a length of 43.8 ± 6.6 nm. Although these samples exhibited distinct sizes and shapes, impressive packing behaviors were observed in that two-dimensional arrays were easily observed by TEM. Interestingly, individual silver nanoparticles were not in direct contact with each other because residual CTAB adsorbed on the surface provided steric hindrance, which prevented their coalescence or aggregation during their formation stage in solution. As a result, after the nanoparticles were retrieved and dried, their relatively uniform size distribution enabled an orderly-packed arrangement because of the weak van der Waals attraction among them. In addition, every particle can be reasonably concluded to have existed as a single crystal. Moreover, the notable color contrast among them was caused by uneven TEM grid that led to minute misalignment of incident electron beam along crystallographic planes of selective nanoparticles.

The morphology of the silver nanoparticles is determined by the relative concentrations of the ingredients involved because nucleation and growth are the primary formation steps. Literature reports have established that the separation of nucleation and growth is critical for the fabrication of monodispersed nanoparticles [23–25]. The separation of nucleation and growth can be realized by LaMer's concept of "burst nucleation", where numerous nuclei are produced simultaneously followed by diffusional control of growth without further nucleation [26]. To synthesize silver nanoparticles, a large molar ratio (CTAB/silver cations>2.5) is essential in directing the reaction toward the formation of cubic nanoparticles rather than spherical nanoparticles [27]. In our samples, we fixed the ratio at 3 so that the formation of nanocubes was expected. Qualitative understanding of size variation among these samples can be rationalized by the molar ratio between glucose and silver cations (glucose was used as a reducing agent). At a ratio of 1.5 (sample SC), the silver cations were readily reduced to reach a supersaturation state for numerous nuclei to form and compete for growth. As a result, the silver nanoparticles appeared in both cubic and spherical forms with a slightly broader size distribution. In contrast, when a subdued ratio of 0.1 was used (sample SA), inadequate glucose inhibited the reduction of silver ions; hence only a limited number of nuclei became available. This limited number of nuclei allowed the CTAB to affect the growth rate via its anisotropic adsorption behavior. Therefore, the resulting silver nanocubes exhibited truncated edges and rounded corners with a relatively narrower size distribution. For sample SB, which was prepared at a ratio of 0.35, the concentration of glucose was sufficiently high to initiate the "burst nucleation", but the

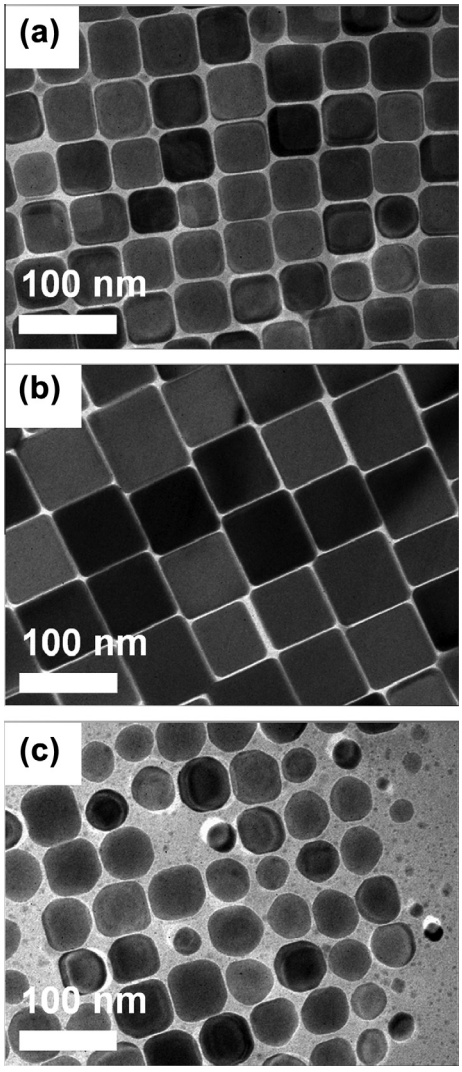

Fig. 1. TEM images of samples (a) SA, (b) SB, and (c) SC, respectively.

number of nuclei was still insufficient. Hence, we observed slightly larger but well-defined silver nanocubes instead. Notably, the formation of micelles in aqueous solutions using CTAB is known to affect the shape and size distribution of the resulting metal nanostructures [22]. According to product information from Sigma–Aldrich, the critical micelles concentration for CTAB in water is typically between 0.92 and 1 mM. In our formulation, the CTAB concentration was kept at 50 mM. Hence, the functioning of CTAB in different samples might also contribute to the observed variations in size and in standard deviation. Notably, in surfactant-assisted synthesis, the primary role played by the surfactant is its anisotropic adsorption on selective crystallographic planes to promote/retard their growth into unique shapes; the secondary effect is the interaction of micelles with the nuclei that affect the growth process [22]. In our case, we were unable to clearly identify the effect of micelle formation on the shape and size of the silver nanoparticles because the interaction between the micelle and silver nuclei was very subtle and complicated.

The size variation among our samples can also be approached from a quantitative standpoint. Because the glucose/silver cation ratios were less than 1 in both samples SA and SB, the amount of glucose became the limiting factor for silver nucleation and growth. The glucose ratio between sample SA and SB (i.e., SB/SA) was 3.5. Hence, the expected edge-length ratio for the synthesized samples (SB/SA) was 1.52 (the cubic root of 3.5). This value is in reasonable agreement with the results of our measurements; 1.44 (70.9 nm/49.3 nm). In the case of sample SC, the glucose was present in excess, and its oxidation produced protons that etched the freshly-formed silver nanoparticles. Therefore, the resulting nanoparticles exhibited somewhat random shapes and their sizes were smaller than those of the nanoparticles in sample SB.

Fig. 2a shows a truncated silver nanocube from sample SA, and its selective area electron diffraction pattern is presented in Fig. 2b. Apparently, the diffraction pattern confirmed a single crystalline phase with diffraction planes identified as the (200) and (220) planes. A high-resolution image of this sample is provided in Fig. 2c, which reveals a lattice spacing of 0.198 nm. This value is consistent with that expected for the (200) plane in a fcc silver phase. Therefore, we realize that the six facets on the silver nanocubes are {200} planes. According to the results reported by Sun and Xia, after the Miller indices for the six facets have been determined as {200} planes, crystallographic orientation suggests that the rounded edges are {110} planes and that the truncated corners become {111} planes [20]. Notably, the atomic arrangement for the (200) planes in a fcc lattice is identical to that of (100) planes. Hence, we conclude that the sample SA contains (100) planes on six facets with (110) and (111) planes appearing on the edges and corners, respectively.

To validate the Miller indices for the exposed planes and their relative abundance, we obtained X-ray diffraction (XRD) patterns (shown in Fig. 3) and compared the diffraction intensity of selected planes to that of standard fcc silver (JCPDF: 04-0783). In ideal isotropic fcc silver, the (111) plane is the strongest peak and the intensity ratio of (111)/(200) is expected to be 2.5. Interestingly, for sample SB, which adopted a perfect cubic shape, the (111) peak was negligible, whereas the predominant signal was due to the (200) plane. This result confirmed that the six facets were indeed (100) planes. Moreover, the ordered two-dimensional packing of nanocubes was presumed to strengthen the (200) signal considerably. In contrast, in the case of samples SA and SC, the (111)/(200) ratio was 1.4 and 1.9, respectively. Despite the observation of (111) plane, these values were still less than value of 2.5 for the isotropic structure. This result implies that the (111) plane was under-represented in our samples. In the case of the truncated nanocubes of sample SA, we also observed the (220) diffraction

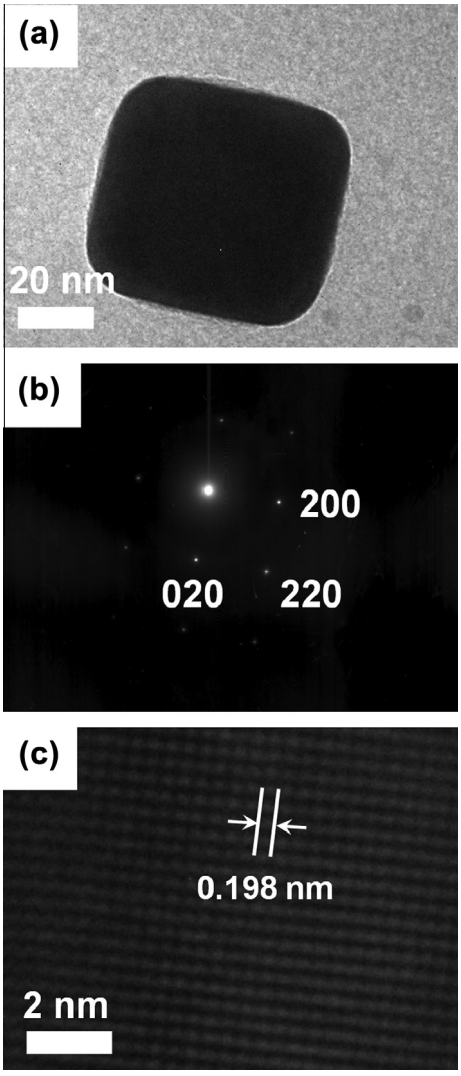

Fig. 2. (a) TEM image of a truncated nanocube from SA, (b) its selective area diffraction pattern, and (c) a high-resolution image with lattice spacing identified.

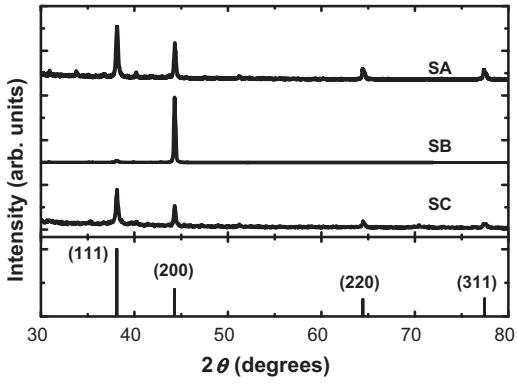

Fig. 3. XRD patterns of samples SA, SB, SC, and that of standard JCPDF 04-0783.

peak. We believe that the simultaneous presence of the (111), (200), and (220) planes substantiates that the morphology of this sample is truncated compared to a well-defined nanocube, which would only produce a strong (200) signal. However, the (111)/(200) ratio in the case of sample SA, 1.4, was slightly higher than what we expected. However, in the case of sample SC, which included cubic, spherical, and irregular-shaped nanoparticles, we

expected (111), (200), and (220) planes to be observed simultaneously. In addition, its (111)/(200) ratio was closer to that of bulk silver.

Notably, the XRD measurements were performed on samples in powder forms, and the diffraction patterns indicated preferred orientations of selective planes. This behavior was anticipated and was consistent with the sample morphology. Indeed, in an ideal powder case, the XRD pattern is expected to show a random orientation similar to that of a polycrystalline material. However, in our case, the silver nanocubes and truncated nanocubes were easily assembled because of their uniform sizes and morphologies. This orderly packing (shown in Fig. 5) strengthened the XRD signals from certain crystallographic planes; consequently, the XRD patterns of SA and SB showed rather strong preferred orientations.

Metallic nanoparticles are also known to exhibit unique absorption peaks in the visible regime; these peaks are associated with plasmon resonance from free surface electrons. In the literature, the plasmon resonance absorption has been reported to be affected by several factors, including the size, composition, morphology, and aggregation of the nanoparticles, and the type of solvent used [28–30]. Hence, nanoparticles with distinct shapes are expected to exhibit characteristic absorption patterns that should facilitate their quick identification. Fig. 4 presents the UV–visible absorption spectra for our samples. For both nanocubes and truncated nanocubes, the recorded absorption peaks were in agreement with results previously reported in the literature, with minor deviations associated with variations in the particle size and in the dielectric constant of the solvent. As shown, the truncated nanocubes (sample SA) produced absorption peaks at 349, 391, and 471 nm. According to the literature, quadrupole local surface plasmon (LSP) is responsible for the strongest peak at 471 nm, whereas a mixed effect of dipole and quadrupole LSP renders weaker absorptions at 349 and 391 nm [31,32]. In the case of the nanocubes in sample SB, four notable absorption peaks at 346, 414, 506, and 581 nm, were observed. Earlier report by Cobley et al. indicated that the strongest peak at 506 nm is associated with quadrupole LSP, whereas the signal at 581 nm is caused by dipolar LSP [32]. In addition, the smaller peaks at 346 and 414 nm were induced by a mixed effect of dipole and quadrupole LSP. In the spectrum of sample SC, a broad absorption peak at approximately 443 nm appeared, which indicated an irregular shape and a relatively large size distribution. The TEM image showed that, sample SC consisted of nanoparticles with cubic, spherical, and irregular shapes. Consequently, their characteristic plasmon resonance peaks likely overlapped to some degrees, thereby resulting in a broad absorption pattern.

The zeta potential of the as-synthesized silver nanoparticles is critical because its magnitude strongly affects the stability of the suspended silver colloids. The zeta potentials of samples SA, SB, and SC, were −21.67, −22.44, and −27.17 mV, respectively. Fig. 5 shows the SEM images of our samples. As shown, silver nanocubes and truncated nanocubes synthesized in this work were indeed present in large quantities, and their size distributions were relatively uniform. In addition, they were readily assembled without undesirable coalescence and aggregation. These SEM images provide solid evidences that our water-based formula is effective in the facile production of large-quantity nanocubes and truncated nanocubes with a reduced size distribution. On the basis of the SEM images, the yields for SA and SB were estimated to be greater than 95%. However, due to its irregularly shaped particles, the exact determination of the yield for sample SC was not meaningful.

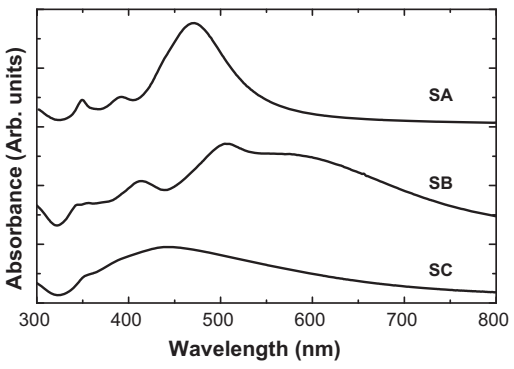

Fig. 4. UV–visible absorption profiles for samples SA, SB, and SC.

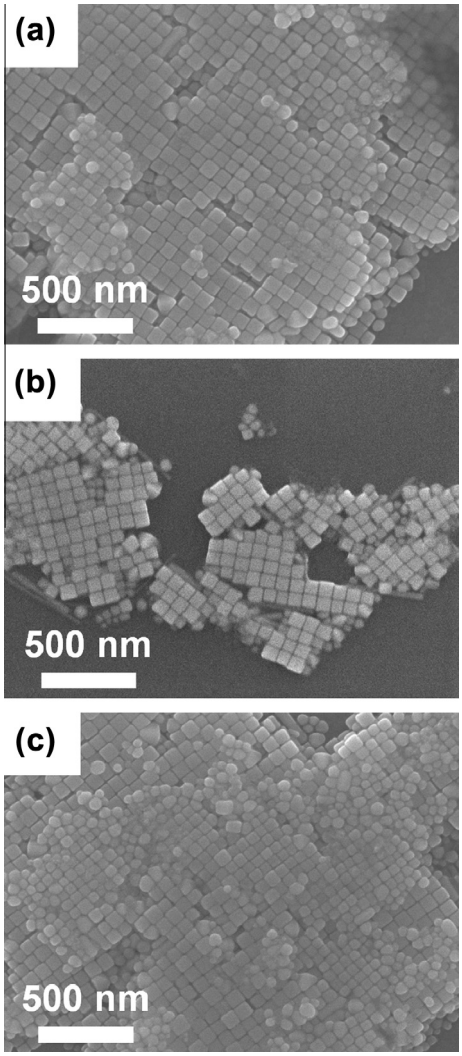

Fig. 5. SEM images of samples (a) SA, (b) SB, and (c) SC.

4. Conclusions

We developed a water-based hydrothermal synthetic approach to prepare monodispersed truncated silver nanocubes in large quantity. The fabrication scheme involved CTAB as a surfactant in conjunction with glucose as a reducing agent to reduce silver complexes. Using an optimized formula we were able to obtain truncated silver nanocubes with an edge length of 49.3 nm; these nanocubes exhibited (100), (110), and (111) planes on the facets, edges, and corners, respectively.

Acknowledgement

Financial support from National Science Council of Taiwan is greatly appreciated (NSC100-2221-E009-075-MY3).

References

[1] D.L. Feldheim, C.A. Foss, Metal Nanoparticles; Synthesis, Characterization, and Applications, Marcel Dekker, New York, 2002.
[2] F.R. Fan, D.Y. Liu, Y.F. Wu, S. Duan, Z.X. Xie, Z.Y. Jiang, Z.Q. Tain, J. Am. Chem. Soc. 130 (2008) 6949.
[3] A. Vaškelis, A. Jagminienė, L. Tamašauskaitė–Tamašiūnaitė, R. Juškėnas, Electrochim. Acta 50 (2005) 4586.
[4] S. Tokonami, Y. Yamamoto, H. Shiigi, T. Nagaoka, Anal. Chim. Acta 716 (2012) 76.
[5] M.A. Bratescu, O. Takai, N. Saito, J. Alloys Comp. 562 (2013) 74.
[6] X. Wang, Y. Lin, F. Gu, Z. Liang, X.F. Ding, J. Alloys Comp. 509 (2011) 7515.
[7] L.M. Forbes, A.P. Goodwin, J.N. Cha, Chem. Mater. 22 (2010) 6524.
[8] N.V. Long, T.D. Hien, T. Asaka, M. Ohtaki, M. Nogami, J. Alloys Comp. 509 (2011) 7702.
[9] V.K. Sharma, R.A. Yngard, Y. Lin, Adv. Colloid Interface Sci. 145 (2009) 83.
[10] A.R. Tao, S. Habas, P. Yang, Small 4 (2008) 310.
[11] K. Ni, L. Chen, G. Lu, Electrochem. Commun. 10 (2008) 1027.
[12] J. Zhao, Z. Zhang, S. Yang, H. Zheng, Y. Li, J. Alloys Comp. 559 (2013) 87.
[13] J. Henzie, M. Grünwald, A. Widmer-Cooper, P.L. Geissler, P. Yang, Nat. Mater. 11 (2012) 131.
[14] T. Dadosh, Mater. Lett. 63 (2009) 2236.
[15] Y. Yang, S. Matsubara, L. Xiong, T. Hayakawa, M. Nogami, J. Phys. Chem. C 111 (2007) 9095.
[16] J. Zhang, M.R. Langille, C.A. Mirkin, Nano Lett. 11 (2011) 2495.
[17] S.H. Im, Y.T. Lee, B. Wiley, Y. Xia, Angew. Chem. Int. Ed. 44 (2005) 2154.
[18] P. Christopher, H. Xin, S. Linic, Nat. Chem. 3 (2011) 467.
[19] M. Szymańska-Chargot, A. Gruszecka, A. Smolira, K. Bederski, K. Gluch, J. Cytawa, L. Michalak, J. Alloys Comp. 486 (2009) 66.
[20] Y. Sun, Y. Xia, Science 298 (2002) 2176.
[21] D. Yu, V.W.W. Yam, J. Am. Chem. Soc. 126 (2004) 13200.
[22] X. Ye, L. Jin, H. Caglayan, J. Chen, G. Xing, C. Zheng, V. Doan-Nguyen, Y. Kang, N. Engheta, C.R. Kagan, C.B. Murray, ACS Nano 6 (2012) 2804.
[23] V.K. LaMer, R.H. Dinegar, J. Am. Chem. Soc. 72 (1950) 4847.
[24] Z.A. Peng, X. Peng, J. Am. Chem. Soc. 124 (2002) 3343.
[25] X. Peng, J. Wickham, A.P. Alivisatos, J. Am. Chem. Soc. 120 (1998) 5343.
[26] J. Park, J. Joo, S.G. Kwon, Y. Jang, T. Hyeon, Angew. Chem. Int. Ed. 46 (2007) 4630.
[27] K.S. Birdi, Handbook of Surface and Colloid Chemistry, second ed., CRC Press, 2003.
[28] E. Hutter, J.H. Fendler, Adv. Mater. 16 (2004) 1685.
[29] J.Z. Zhang, C. Noguez, Plasmonics 3 (2008) 127.
[30] J.A. Scholl, A.L. Koh, J.A. Dionne, Nature 483 (2012) 421.
[31] D.D. Evanoff Jr, G. Chumanov, Chem. Phys. Chem. 6 (2005) 1221.
[32] C.M. Cobley, M. Rycenga, F. Zhou, Z.Y. Li, Y. Xia, J. Phys. Chem. C 113 (2009) 16975.